KERNFORSCHUNGSZENTRUM

KARLSRUHE

Institut für Material- und Festkörperforschung

The technology of UAl_3-Al irradiation test plates

S. Nazare, G. Ondracek, F. Thümmler

KERNFORSCHUNGSZENTRUM KARLSRUHE

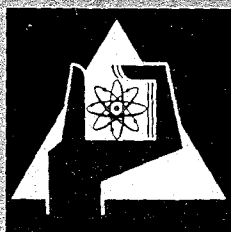April 1967   KFK 585

Institut für Material- und Festkörperforschung

The technology of UAl_3-Al irradiation test plates

von

S.Nazaré, G.Ondracek, F.Thümmler

Gesellschaft für Kernforschung m.b.H., Karlsruhe

List of contents

1. Introduction

Since some time reactors are being built with the objective of producing a high and uniform neutron flux ($>$ 10^{15} n/cm^3 sec). Very high neutron fluxes are required for the production of transuranium elements as well as for neutron physics experiments [1,2]. These can be attained by increasing the fuel concentration in the fuel element and the U^{235} enrichment of the fuel. However, both factors increase the heat production, (as is illustrated on the basis of three Materials Testing Reactors in fig. 1). The high thermal flux practically dictates the use of thin plate-type dispersion fuel elements, with a metallic matrix. Also the demands on the cladding and construction materials in the fission zone are increased.

The requirement for a high fuel concentration in the A.T.R. is fulfilled through the use of a U_3O_8-Al dispersion instead of the commonly used U-Al alloy. Inspite of its good operational behavior, the U_3O_8-Al system cannot - for various reasons - be looked upon as optimal. With higher neutron and thermal fluxes, and the resulting higher operating temperatures, a fuel with a higher thermal conductivity and better compatibility with the matrix is desirable to ensure a trouble-free operation.

A satisfactory irradiation behavior requires an intact contact surface between the fuel particles and matrix. The

continuity of the matrix can be interrupted by reaction product zones, recoil zones, and fission gas agglomeration. To prevent such discontinuities, and depending on the type of dispersions, limits are imposed on the fuel concentration and operational temperatures. The dispersed fuel particles should not fall short of a minimum size [27].

The possibility of increasing the flux by increasing the concentration has limits imposed by technology. The rolling of plate type fuel elements with concentrations higher than a certain figure presents problems. Finally, the distribution of the fuel and a burnable poison in the matrix should be very uniform. Although no detailed investigations on this point, at least for U_3O_8-Al and UAl_3-Al dispersions, have been reported to date, this factor is certainly of importance. From this point of view, it appears that powder metallurgical processes are in general preferable to melting methods.

In view of the above considerations, it seems that uranium-aluminide dispersions in aluminium approach an optimal fuel system on aluminium basis. UAl_2 is highly pyrophoric and unstable. The UAl_4 phase has the lowest uranium content and its preparation in the desired form is not established. The following investigations deal with the combination UAl_3-Al. The produced fuel plates should be of a quality desirable in irradiation experiments. Their technology could eventually be used as a basis for production of fuel elements. It is possible that such fuel elements may be considered for later use in the French-German High Flux Reactor.

2. Literature review

2.1 Preparation of UAl_3

The uranium-aluminium constitutional diagram in fig. 2 shows so far as is now known, no evident homogenity for UAl_3 [4]. The slightest variation in the stoichiometrie will therefore result in the presence of either one of the neighbouring phases. Such variations are, however, when melting processes are used, difficult to prevent, because the vapour pressure of uranium is much lower than that of aluminium. At the peritectic transformation temperature of UAl_3, the ratio of the vapour pressures is about 10^7 ($P_{Al} : P_U = \frac{10^{-2}}{10^{-9}}$ Torr) [5], [6].

The formation of the highly pyrophoric UAl_2 phase is very undesirable, for it is the main cause of uraniumdioxide impurities in the aluminides. The temperature function of the free energy of reaction for the three known aluminides [33], [34] are:

$$\Delta G_{UAl_2} = -27.4 + 21.10^{-3} \, T \text{ (Kcal)} \tag{1}$$

$$\Delta G_{UAl_3} = -32.9 + 13.10^{-3} \, T \text{ (Kcal)} \tag{2}$$

$$\Delta G_{UAl_4} = -41.5 + 9.9.10^{-3} T \text{ (Kcal)} \tag{3}$$

Further available thermodynamic data on UAl_3 are the standard entropy ($S\,298 = 32.5$ cal/$^\circ$C) and the standard enthalpy ($H_{293} = -25.2 \pm 2.2$ Kcal/Mol).

Until the present time UAl_3 has been prepared by the following
three methods:

a) Induction or arc melting of uranium-aluminium mixtures

b) Reaction of uranium-hydride or fluoride with aluminium powder

c) Hot-pressing of uranium aluminium mixtures

Induction melting is carried out in graphite crucibles, at
times with a coating of magnesium-zirconite. After melting
and superheating (800 ^{o}C) the pure strip aluminium in vacuum
or air, stoichiometric amounts of uranium are added. After
completion of the reaction, the melt can be poured in pre-
heated steel moulds or graphite moulds coated with magnesium-
zirconite [7,8,9].

In arc melting with water cooled copper crucibles, the stoi-
chiometric mixture of uranium and aluminium is heated
simultanously in inert gas or vacuum (5 x 10^{-3}Torr). The
regulus is repeatedly melted (8 to 10 times) to complete
the reaction and produce homogeneous melts [8, 30]. In either
process, the incongruent melting of UAl_3 can be overcome to a
great deal by sufficient annealing below the peritectic
temperature.

In the uranium hydride reaction with aluminium [8,10,11,30],
pure uranium is hydrided with highly pure hydrogen. The pure
hydrogen can, for example, be produced by decomposing uranium
hydride. The uranium-hydride is then mixed with a stoichiome-
tric amount of aluminium powder (particle size < 44 μm, de-
gassed in vacuum at 560 ^{o}C for 4 hours). The reaction takes
place in vacuum or in an argon atmosphere.

Aluminium oxide or graphite crucibles were used. The reaction begins at 6oo $^{\circ}$C, the temperature thereby rises to about 1ooo $^{\circ}$C, and is maintained at this level for a long period of time (about 16 hours) to guarantee a complete reaction. The process can be accelerated by hot pressing the mixture (1ooo $^{\circ}$C; 3,5 Mp/cm^2; 2 hours) . In a similar process but under modified conditions (9oo $^{\circ}$C - 12oo $^{\circ}$C; 1 atm), the primary substance used is uranium fluoride [37]. The reaction produces uranium-aluminide and aluminium monofluoride. The aluminium monofluoride is be subsequently separated by vacuum distillation at 12oo $^{\circ}$C.

In the third available method for the preparation of UAl$_3$, uranium and aluminium strip-mixed in stoichiometric proportions is hot pressed at 6oo $^{\circ}$C [3]. The pellets so formed are subsequently annealed at 95o $^{\circ}$C in vacuum. It is, however, possible to use stoichiometric powder mixtures as well (U < 44 μm ; Al > 23 μm < 1o3 μm). These can be either mechanically mixed powders e.g. by tumbler movement 5o R.p.m. for 15 minutes under helium, or coated particles. U-Al alloys (25 wt% U) have been, for example, prepared by hot pressing at 45o $^{\circ}$C spherical uranium powder (mean particle size of 7o μm) coated with aluminium [15].

The methods described above yield a porous mass that can be easily ground under argon. Ignition of the powders during grinding can be prevented by using an inert gas (argon) or a protective liquid petrolether [8,16,17,3o]. In some cases, the final product is annealed once again for degassing and homogenising (5oo - 9oo $^{\circ}$C; 3 - 1o hours). The best product,

judged by its chemical analysis, is obtained through the hydride process. Its characteristics are given in fig. 3.

2.2 Production of UAl_3-Al pellets

The option is once again between melting and powder metallurgical techniques. In the former case, the distribution of the aluminide in the ingot is not uniform due to gravity segregation. The uranium content also varies from batch to batch. Such alloys - generally dispersions of UAl_4 or UAl_3 in Al - have been prepared with relatively high uranium content without resorting to the previous production of UAl_3, as follows: [18,19,2o,24,25,26]. Aluminium is superheated in stationary or rotating graphite crucibles to 98o ^{o}C in helium; uranium is added, and the temperature raised to 14oo ^{o}C. The melt is stirred with a stream of helium (38o Torr), and poured in cooled graphite moulds.

The powder metallurgical method allows a much better control of the distribution, composition, and shape of the dispersed aluminide phase. The UAl_3 and Al (mainly $>$ 44 μm) powders are mixed mechanically, e.g., in glas containers, at times with enclosed aluminium spheres [1o,11,2o]. The configuration of the mixing containers and the number of the enclosed aluminium spheres seem to have no influence on the quality of the mixtures. Mixing is carried out in air and argon ($\sim$3 hrs); moisture is to be avoided during mixing.

The powder mixtures are compacted by pressing and sintering [7,9,17,21]. The applied pressure is either one sided, two sided, (4.6 - 7.8 Mp/cm^2) or isostatic (7 Mp/cm^2). The die lubricant is stearic acid in methanol. The sintering temperature (450 - 600 °C) and sintering times (4-96 hours) can be varied broadly [7,17]. The attained densities (75-85% theoretical density) are based on the theoretical density of the UAl$_3$-Al compact. In practice, reactions - at least to a small degree - are likely to take place between UAl$_3$ and Al leading to the formation of UAl$_4$. The stabilization of UAl$_3$ is possible through the addition of silicium, germanium, palladium, magnesium, zirkonium and tin (o.3 - 3 wt% o) [24]. On the other hand, such additions are likely to complicate the recovery of the spent fuel.

The fabrication of UAl$_3$-Al green pellets to Al clad fuel elements is mainly carried out by roll bonding through the picture frame technique [7,29,3o]. The cover plates and the picture frame material is Al 6o61-F or Al 6o61 clad on one or both sides respectively with pure aluminium (5%). The composite plate is held together with 2 rivets. After cleaning and pickling the cover plates and picture frame with 5o % HNO$_3$, the UAl$_3$-Al core (< 55 wt% UAl$_3$ - o.19 wt% B$_4$C - Al) is fitted in the frame and the composite plate riveted together. The rolling can be carried out on batches of up to 9 plates. The plates are preheated (5oo°C, 45 minutes) and annealed (5oo °C, 5 min) between passes. The reduction per pass is 2o %. The hot rolling is carried out up to a thickness of about 1.4 mm. Subsequent cold rolling is used to attain the desired final

dimensions. Cold rolling also levels the plates. Radiography
is used to mark the cores; the plates are sheared to end
dimensions, rolled level, and cleaned. Blister tests can be
made between rolling passes to control bonding.

Attempts have also been made to clad prepressed uranium-
aluminium powder mixtures by electronically welding in cap-
sules followed by extrusion at low temperatures and speeds
[31].

2.3 Structure and properties of UAl_3-Al dispersions

The uranium-aluminium equilibrium diagram (fig. 2) shows
practically no solid solubility of uranium in aluminium.
New investigations, however, suggest a small solubility
[22]. The grain structure of the components in the disper-
sion can be coarse or fine depending on the heat treatment.
Hot pressed powder mixtures are, as expected, fine grained
[15]. The metallographic analysis can be carried out with
the help of the following etching procedure [7,24,28]:

a) Electrolytic etching

Electrolyte: 1 part chromic acid (4o%) + 1 part acetic
             acid (5o%) - 1 to 3 min with o,o5 Amp/cm^2

b) Chemical etching

Nitric acid (5o%), 1 minute.

The electrolytic etch yields typical colours for the various aluminides:

- UAl_2 appears white or bluish

- UAl_3 appears yellow or orange

- UAl_4 appears bluegrey or grey

Both components, UAl_3 (density 6.8 g/cm^3) and Al (density 2.7 g/cm^3) have a cubic lattice [8]. The lattice parameter for aluminium at room temperature and the temperature function of the lattice parameter of UAl_3 is given in fig. 4. The lower part of the curve (till 3oo $^\circ$C) can be expressed by the equation:

$$a_{UAl_3}(T) = 4.2536 + 7.1667 \times 10^{-5}T \; (\text{Å}) \tag{4}$$

the upper part (3oo-75o$^\circ$C) by the equation:

$$a_{UAl_3}(T) = 4.2855 + 5.7854 \times 10^{-5}(T-3oo) + 6.68 \times 10^{-8}(T-3oo)^2$$
$$+ 1.97 \times 10^{-1o}(T-3oo)^3 \; (\text{Å}) \tag{5}$$

The thermal properties of UAl_3-Al dispersions are not reported in the literature, although such data are available for the components themselves. The data are summarized in fig. 5 [12,32].

The available data on the mechanical properties restrict themselves to Al clad fuel elements [33,34,35]. Tensile and

yield strength measurements have been carried out for two
UAl$_3$ concentrations (34 and 5o wt%). The specimens were clad
with the following 2 types of aluminium Al-1ooo and Al-X 8oo1.
In fig. 6, the tensile and yield strengths are plotted. From
this data, and the dimensions of the specimens (total plate
cross-section = 1.27 x 5.86 mm = o.74 cm^2; UAl$_3$-Al core cross-
section = o.51 x 58 mm = o.29 cm^2), it is possible to evaluate
the temperature function of the UAl$_3$-Al core strength without
the cladding. In the simplest case it can be postulated that:

$$\sigma_G = \frac{\sigma_{Al} \times q_{Al} + \sigma_D \times q_D}{q_G} \qquad (kp/cm^2) \qquad (6)$$

wherein:

σ_D = tensile strength of the dispersion
σ_G = total tensile strength of the core and cladding
σ_{Al} = tensile strength of the cladding
q_{Al} = relative cross-section of the cladding
q_D = relative cross-section of the core
q_G = relative cross-section of the composite plate

The so calculated values of σ_D are also plotted in fig. 6.
It can be seen that at higher aluminium concentrations the
temperature dependance of the tensile strength and tensile
strength itself is, as expected, greater than that of alumi-
nium alone. The bond between the dispersed UAl$_3$ particles
and the Al-matrix should nevertheless be such that the load
is distributed over the total dispersion and not only on the
matrix. If this is not the case, the values for the dispersion,
independent of temperature, would lie below those for the
Al-matrix.

The values of tensile strength for the core obtained by
using the above equation (6) are the lowest values. In fact,
the values for the UAl_3-Al core are probably higher. This
can be deduced by considering the phenomenon of fracture
(see fig. 7). The measured tensile strength values or the
calculated values for the ultimate load on the composite
plate are greater than the ultimate load on the cladding. On
the other hand, the ultimate elongation of the cladding is
greater. The rupture of the core therefore takes place at
the point where the elongation values correspond to the
ultimate load of the composite plate. At this stage, the
cladding elongates further - the load decreases - to attain
the elongation corresponding to the increased load (greater
than the ultimate load of the cladding alone) suddenly brought
upon it due to the rupture of the core.

Since the calculations with equation 6 are based on the known
ultimate load values of the Al-cladding, the deduced tensile
strength values for the core are too low. The real value of
the tensile strength for the core would be equal to the
calculated, only if the cladding and core fractured simulta-
neously. Otherwise the real tensile strength values for the
core could be greater than those calculated.

3. Experimental work

3.1 Preparation of UAl$_3$ by melting technique

In the following investigations the melting technique was
chosen to prepare UAl$_3$ for the following reasons:

As can be seen in fig. 3 the hydride reaction method of pre-
paring UAl$_3$ and its subsequent grinding results in very fine
powders. It is, however, aimed to achieve a coarser ($>$ 6o μm)
UAl$_3$ particle size in the dispersion. In addition, the in-
ductive melting is technically easy to accomplish, even on
a large scale basis. Finally the hydride process involves
the risk of higher gas contents.

Initial experiments were undertaken to find out which crucible
material was most suitable to melt pure compounds.

Three crucible materials were investigated:
- graphite with MgZrO$_3$ coating (Metco process)
- graphite with Al$_2$O$_3$ coating (Metco process)
- Al$_2$O$_3$ without high temperature annealing
- Al$_2$O$_3$ with high temperature annealing

The melt charges consisted of about 15o g of uranium and
aluminium strip. The conclusion that could be drawn was
that magnesium zirconite dissociated at high temperatures
($>$ 15oo^{o}C):

$$MgZrO_3 \xrightarrow{> 15oo^oC} MgO + ZrO_2 \qquad (7)$$
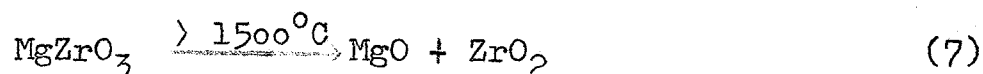
The zirconium oxide (vap. press lo^{-8} Torr) remains in the

melt. Magnesium oxide, on the other side, evaporates and condenses on the walls of the recipient. These results have been confirmed by X ray analysis. Graphite with $MgZrO_3$ coating is, therefore, not a very suitable crucible material. The Al_2O_3 coatings on graphite have also an important draw-back. They do not withstand a strong thermal shock during heating and cooling. The resulting cracks can lead to a direct reaction between the melt and graphite. In addition the coating flakes falling in the melt produce insoluble impurities, leading to the conclusion that Al_2O_3 does not react with the melt at the operating temperatures.

It was therefore obvious to use Al_2O_3 crucibles which were satisfactory, provided they were annealed in high vacuum (10^{-5} Torr; $1550^{\circ}C$). When not annealed, the silicium-rich binder of the crucible reacted with the melt (fig.8).

Subsequent experiments for the preparation of UAl_3 were therefore carried out in annealed Al_2O_3 crucibles. The charges consisted of thick uranium chips and aluminium strip. The uranium was always placed above the aluminium in the crucible. Other geometrical shapes, e.g., cylindrical uranium and aluminium rods have no influence on the resulting UAl_3 product. The uranium was rinsed with acetone and carbon tetrachloride and pickled in a mixture of nitric and acetic acids.

The required composition of the charge was determined empirically. A lower percentage of uranium is required to compensate the evaporation losses of aluminium. With various charges (50-800 g) and with stationary crucibles, it was found that

the amount of excess aluminium should be such as to produce 7 % of the UAl_4 phase. This calculation is made with the help of the equilibrium diagram assuming no aluminium losses due to evaporation. The following melting procedures appear desirable:

atmosphere	helium, 4oo Torr
heating rate	$\sim 5o$ $^{o}C/min$
maximum temperature	16oo ^{o}C
rapid cooling	(3o $^{o}C/min$) from the maximum to homogenising temperature
homogenising	125o ^{o}C, 5 hrs
cooling	optional

The helium pressure plays a role in preventing a possible dissociation of UAl_3 in vacuum () lo^{-4} Torr;) 12oo ^{o}C).

The first step to determine the extent of UAl_2 segregation was to cut the regulus. UAl_2 has a higher density (2o%) than UAl_3. No segregation could be detected between the top and bottom or the centre and the periphery. The chemical analysis of a specimen near the periphery showed a slightly lower aluminium content (25,85 wt%) than that of a specimen near the centre (26.1 wt%).

Further investigations were metallographic and microprobe analyis. The microstructures (fig. 9) show clearly that the remaining melt has gathered between UAl_3 grains and solidified. From the constitutional diagram the phase between the grain boundaries

can be a peritectically formed UAl_4, or if this reaction is
slow, an eutectic of UAl_4 and Al. The characteristic X-ray
radiation of Al (figs. 1o a and b) and U (figs. 1o c and d)
was monitored. The grain boundaries show an increase or
decrease in aluminium or uranium concentration respectively.
The highest peak in fig.1o a corresponds with the intensity
of pure Al. The amount of the second phase was too small to
be detected by X-ray diffraction, which showed the presence
of a single phase.

The regulus was ground with a hammer mill using a disc and
a ring as inserts. The grinding process is of great importance
since relatively narrow limits are imposed on the UAl_3 particle
size to ensure an optimal behaviour of the dispersion. Con-
sidering that the distance between the dispersed particles
should be greater than two times the thickness of the recoil
zone, the necessary particle size can be mathematically deduced
and graphically illustrated for an ideal dispersion (fig. 11).
Accordingly, with an Al-matrix (path of the fission fragments =
thickness of the recoil zone = 13.7 μm) and the desired UAl_3
concentration (25.89 vol%), the recoil zones would not touch
with relatively coarse UAl_3 particles of 67 μm. Investigations
on the kinetics of the reaction UAl_3-Al $\longrightarrow$ UAl_4 and measure-
ments of the resulting volume changes can later produce a
value for the reaction zones. The importance of such minimum
particle size calculations is still an open question,
however, for the UAl_3-Al system. The dispersed particle size
has an upper limit, too (probably 125 μm), since too coarse

particles are likely to be damaged and ground during rolling. This would lead to an uneven and uncontrollable fuel distribution in the matrix.

In order to grind the UAl_3 in such a way as to produce large amounts of the desired particle size, the optimal grinding conditions have to be determined. The preliminary experimental results are tabulated in fig. 12. Further experiments are in progress. It can, however, be already foreseen that large amounts of the powder fall outside the desired grain class. The coarse fraction ($>$ 125 μm Ø) can be reground - the fine fraction on the other hand has to be sintered or remelted. The lowest temperature required for the sintering of the fine fraction was determined with a dilatometer (fig. 13). The shrinkage of a UAl_3-pellet produced with a pressure of 5 Mp/cm^2 was measured. The first part of the curve so obtained shows an expansion and possible interference caused by degassing and relaxation. Subsequently the expansion and the shrinkage are superimposed, until above a certain temperature the shrinkage becomes predominant. The temperature of the begin of the shrinkage is defined as that where o.2 % shrinkage has taken place [23]. It can be determined by drawing the length of a o.2 % smaller pellet as a function of temperature. The point of intersection of the latter curve with the experimentally determined former curve, gives the temperature of the shrinkage begin (about 96o ^{o}C see fig. 13). It is, in this case, sufficiently low to permit regrinding of the fine fraction after sintering below the peritectic temperature.

The characteristics of the UAl_3 and aluminium powder used in

all the following experiments are tabulated in fig. 14 . The chemical composition of UAl_3 represents a mean value of seven charges. The oxygen is partly present as an oxide.

The lever law permits a calculation of the UAl_3 content of the charge:

$$\frac{(wt\%-Al)\ UAl_4 - (wt\%-Al)UAl_x\ \times\ 100}{(Wt\%-Al)\ UAl_4 - (wt\%-Al)\ UAl_3} = (wt\%-UAl_3)UAl_x \qquad (8)$$

Substitution of the known values for the Al content of UAl_4 (31.19 wt% Al) and UAl_3 (25.37 wt% Al) and transformation yields:

$$\frac{31.19 - \dfrac{100}{\dfrac{(wt\%-U)}{(wt\%-Al)}_{UAl_x} + 1}}{0.0582} = (wt\%-UAl_3)UAl_x \qquad (9)$$

The U/Al ratio $\left(\frac{wt\%-U}{wt\%-Al}\right) UAl_x$ for the UAl_3 is given in fig. 14. Fig. 3 shows the corresponding data for the U.S. product prepared by hydride reaction. Calculation of the UAl_3 or UAl_4 content with equation (9) gives:

	Melting process (IMF)	Hydride process (ORNL)
UAl_3-content (wt%)	93.42	69.19
UAl_4-content (wt%)	6.58	30.81

The UAl_3 content of the U.S. product based on X-ray analysis, given in fig. 3 , is apparently based on the total aluminide

content of the charge.

3.2 Preparation of UAl$_3$-Al pellets and irradiation test plates

The objective is to attain an uniform dispersion of the fuel
in the matrix by mixing UAl$_3$ and Al. Experimental conditions
and results obtained can be seen in fig. 15. The mixing con-
ditions state the ratio of the container volume to powder
volume, since this factor appears to play a role in the
degree of distribution. The determination of the distribu-
tion degree can be either made on pellets or on powder
mixtures. In this case the determination was carried out
on mixtures by chemical analysis.

Considering that the mixture contains x vol% of component A
and y vol% of component B then:

$$\frac{xA}{yB}_{ideal} = \text{ideal weighed in ratio}$$

and

$$\frac{xA}{yB}_{real} = \text{the determined ratio in a sample of}$$
$$\text{a certain weight}$$

Five specimens from the mixture were chemically analysed
each time. The degree of distribution is:

$$v\ (\%) = \left[1 - \frac{(xA/yB)ideal - (xA/yB)real}{\frac{xA}{yB}\ ideal}\right] 100 \qquad (1o)$$

The number of specimens was determined by the consideration
that the scattering of the distribution degree values levels
off above 4 specimens per analysis (fig. 16).

The so determined distribution degree is of course dependent on the size of the specimen per analysis. Statistical considerations, which will be considered in a report to follow, led to the use of a specimen weight of 2 g. The preliminary data - shown in fig. 15 - show that dry mixing with a low ratio of container volume to mixture volume lead to the best results. The wide scattering in the case of wet mixing is due to sedimentative clustering. Further experiments are in progress.

The compacting conditions for one sided pressing of cylindrical as well as two sided pressing of rectangular pellets have been investigated. Fig. 17 shows the variation of density with pressure. The densities attained permit the use of the compacts in the picture frame without resorting to pre-sintering. The density of rectangular pellets increases more rapidly with the pressure. This is due to the geometry of the pellet as well as the use of double acting dies. A significant undesirable variation of the distribution of the UAl_3 in the matrix after compacting are not optically discernible (fig. 18).

The influence of the change in concentration on the pellet density is shown in fig. 19 . The discontinuity in the curve suggests the change over from an aluminide to an Al-matrix.

The question that finally remains to be considered is the density variation within the pellet itself. For this purpose a cylindrical pellet was divided into 3 parts. The density of each part is drawn as a horizontal in fig. 2o . The actual density in the axial direction would then follow the dotted

line. Hardness measurements on a vertical cross-section of a
pellet take, as expected, a course similar to density. The
values plotted are mean values of 4 measurements. Both curves
- density and hardness - have a maximum in the middle. The
hardness values on a transversal cross-section lie on a straight
line. Similar conditions prevail also in the case of rectangu-
lar pellets (fig. 21).

It will be shown later that such density variations do not
influence the quality of the roll-clad irradiation plates.
Very great density variations within the pressed cores of
the picture frames can, however, lead to cracking and dog-
boning during rolling (fig. 22).

The required dimensions of the Al clad irradiation test plates
with UAl_3-Al cores as well as the preliminarily chosen fabri-
cation mode is shown in fig. 23. The composite plates are
held together with 2 rivets on the leading end. The rolls
have to be warmed to avoid temperature gradients during rolling
and to ensure uniform rolling conditions. Unequal heat transport
can lead to different deformations in various sectors of the
plate resulting in warping and distortion. For the same reason
it is important to roll the plates above the recrystalization
temperature of Al ($150^{\circ}C$). On the other hand the temperature
should be such as to avoid the formation of UAl_4, since the
reaction decreases the matrix content and thereby increases the
resistance to deformation. The deformation in the first rolling
pass should be lower (10%) than the subsequent passes (20%).

The rolled plates are straightened by cold rolling and
sheared to end dimensions. Radiography pictures show the
rolled UAl_3-Al cores with cladding (fig. 24). The alignment
of the cores is satisfactory.

In addition to this criterium the bonding between the core
and the cladding is important. This can be judged by a simple
"blister test". For this purpose some test plates were annealed
in air at $5oo^oC$ for 1 hour and checked for blisters. No
blisters could be detected.

3.3 Additional measurements

The coefficients of thermal expansion were also measured with
the view to investigating the difference between the UAl_3-Al
core and the Al cladding. The concentration function was
measured on highly dense (98% T.D.) UAl_3-Al cylindrical pellets
in the temperature range of $2o^oC$ - $5oo^oC$. To avoid the forma-
tion of UAl_4 the chosen heating rate was high (5^oC/min). The
obtained values are shown in fig. 25. It should be noted that
the ratio of the thermal expansion coefficients of the core
and the cladding is though not extensively investigated of
importance for the quality of the plates. If their ratio varies
considerably from unity, stresses result after cooling. These
can lead to warping of the plate, a break in the bond between
the core and the cladding, and, in an extreme case, to cracks
in the core and cladding [38].

UAl_3-Al pellets have also been heated in a dilatometer with
very low heating rates ($o.2$ ^oC/min, for $5o$ hrs) (fig. 26). The

expansion curve shows variations from linearity as a result
of the $UAl_3 + Al \longrightarrow UAl_4$ reaction. Such a reaction is, as is
well known, accompanied by a volume increase ($\sim 1.6\%$). The
reaction seems to achieve a considerable pace at about 480 $^{\circ}C$,
resulting in a maximum variation of length.

Metallographic investigations show complete reaction of UAl_3
to UAl_4 (fig. 27). These results have also been confirmed by
microprobe analysis of the UAl_3-Al-compacts. Obviously one has
to carry out the process at temperatures lower than 480 $^{\circ}C$
to avoid swelling due to reaction. This swelling makes the
fitting of the pellet in the picture frame difficult and
can also lead to defects during hot rolling.

Literature

[1]   Swartout J.A., Bock A.L., Cole T.E., Cheverton R.D.
      Adamson G.M., Winters C.E. A/Conf. 28/P 221, 1964

[2]   Cole T.E., CF-6033 - lo F 3, 1960

[3]   Pearce R.J., Berkeley Nucl. Lab., private Communication
      RDD/BNL/M/RSP/LPC - 9.5.1966

[4]   Hansen M., Constitution of binary Alloys, McGraw Hill
      S.143, 1958

[5]   Brewer L., Searcy A.W., J.Am.Chem.Soc.Vol 73

[6]   Rauh E.G., Thorn R.J., J.Chem.Phys. Vol 22, p. 1414
      19654 and ANL - 5203

[7]   Saller J.A., Progr. in Nucl. Energy, Serie V/9, S.35, 1962

[8]   Gibson G.W., de Boisblanc D.R., Powder Metallurgy
      Conference, New York, 1965

[9]   Graber M.J., Francis W.C., Gibson G.W., Walker V.A.,
      IDO - 16958, 1964

[1o] Private Communication (ORNL- TM - 12oo)

[11] Francis W.C., Gibson G.W., Zsukor M., Graber M.J.
      Zelezny W.F., Moen R.A., IDO - 17154, 1965

[12] Pearce R.J., RD/B/Nr. 451, 1965

[13] Hammond J-P., Adamson G.M. in "Carbides in Nuclear Energy"
      McMillan Co. Ltd., London, S. 648, 1964

[14] Lillie D.E., WASH 12o, 1953

[15] Larson W.L., Fracnis W.C., Gibson G.W., Scarrah W.P.,
      TID-7642, Book 2, 1962

[16] Backensto A.B., Hopson N.F., Lenel F.V., SO-3oo4, 1951

[17] Synder J., Duckworth W.H., BMI-1223, 1957

[18] Hayner W.B., Lorenz F.R., HAPD-PWR-FEM-1o6, 1956

[19] Milko J.H., ORNL-2217, 1956

[2o] Daniel N.E., Foster E.L., Mastry J.A., Bauer A.A.,
      Dickerson R.F., BMI-1183, 1957

[21] Rice W.L.R., TID-11295, Pt. II, S. 1o5, 1964

[22] Saller H.A., Genfer Konferenzberichte, Vol. 9, P. 562
     und P 21, 1956

[23] Ondracek G., Petzow G., Z.Metallkunde Bd. 56, H.8, 1965

[24] Boucher R., J. Nucl. Mat. 1, S. 13, 1956

[25] Dayton R.W., Tipton C.R., BMI 1294/13o1/13o4/13o7, 1958

[26] Thurber W.C., Beaver R.S., Nucl. Metallurgy, S. 57, 1958

[27] White D.W., Beard A.P., Willis A.H., TID-7546, S. 717, 1957

[28] Hills R.F., J.of the Inst.of Metals, Vol.86, S. 438, 1958

[29] Walker V.A., Graber M.J., Gibson G.W., IDO-17157, 1966

[3o] Beißwenger, Ennerst, Grall, Lafaurie, Moneyron, Ondracek,
     Schwartz, Thümmler, HF-Notiz S. 5o, KFZK Karlsruhe,
     IMF, 1966

[31] Meny L., Buffet J., Sauve D., 4. Plansee Seminar,
     S. 566, 1962

[32] Jones T.J., Street K.N, Scoberg I.A., Baird J.,
     Can. Met. Quaterly 2, S. 53, 1963

[33] Gibson G.W., Shupe O.K., 1oo-16727, 1962

[34] Francis W.C., Gibson G.W., Graber M.J., Scarrah W.P.,
     IDO-16857, 1962

[35] Francis W.C., IDO-16827, 1962

[36] Noland R.A., Walker D.E., Hymes L.C., ASTM Special
     Techn. Publ. 276, p. 336, 196o

[37] Seki Y., Mitamura N., Genshiryoku Kogyo, Bd. 11,
     Nr. 9, S. 37, 1965

[38] Tipton C.R., Reactor Handbook, II. Edition, Inter-
     science Publ., N.Y., S. 344, 196o

Reactor		MTR	ETR	ATR
Fuel	Materials	U-Al Alloy	U-Al Alloy	U_3O_8-Al/$_{B_4C}$
	U^{235} Enrich-ment (%)	93	93	93
	U-content (wt%)	18	2o	34.7
Cladding material		11oo Al	11oo Al	6o61 Al
Max.Heat Flux (W/cm^2)		264	41o	6oo
Thermal powder density (MW/l)		o.75	1.2	2.5
Fuel plate surface temperature (^oC)		154	2o4	218

Fig. 1 : Characteristic data of three testing reactors
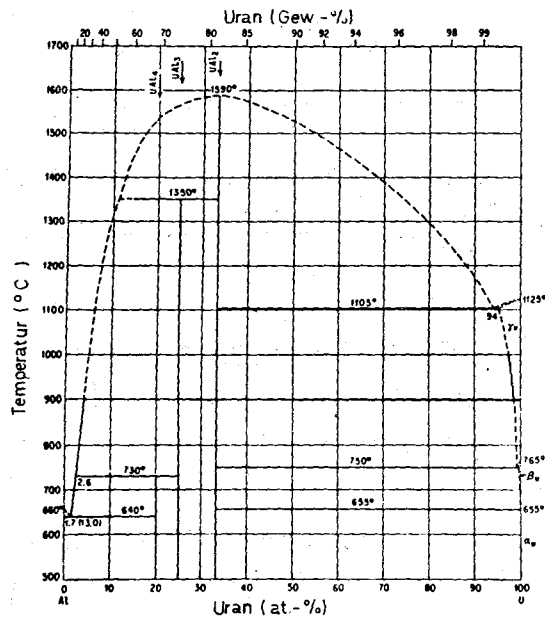
Fig. 2 : The uranium - aluminium equilibrium diagram [4]

Density (g/cm^3)		6.7368
B.E.T. surface (m^2/g)		0.2
Particle size (μm)		3 : 4
U : Al weight ratio		2.68
U Al3 content (wt%) determined by X-ray analysis		95.97
Chemical analysis	O$_2$ (wt%)	0.1627
	N$_2$ (wt%)	0.024
	C (wt%)	0.041
	H$_2$ (wt%)	0.0052
	Rest (wt%)	3.8011

Fig. 3 : Powder characteristics of UAl$_3$ produced by hydride process [10]
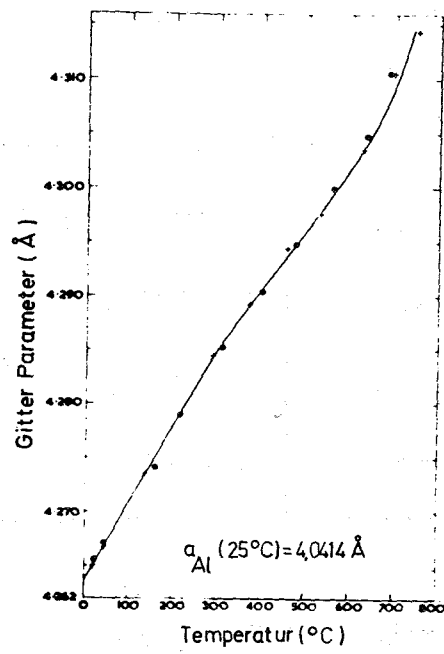
Fig. 4 : UAl₃ lattice parameter as a function
         of temperature [12]

Property	Temperature $^{\circ}C$	UAl_3	Al
Thermal conductivity (cal/sec/ $^{\circ}C$. cm)	65	0.02 ± 0.01	0.541
	200	0.151	0.524
Coefficient of thermal expansion (1/$^{\circ}C$)	0 - 300	1.6809×10^{-5}	2.58×10^{-5}
	0 - 400	1.5898×10^{-5}	2.68×10^{-5}
	0 - 500	1.5214×10^{-5}	2.79×10^{-5}
	0 - 600	1.4945×10^{-5}	2.85×10^{-5}

Fig. 5: Thermal properties of UAl_3 and Al
[12,32]
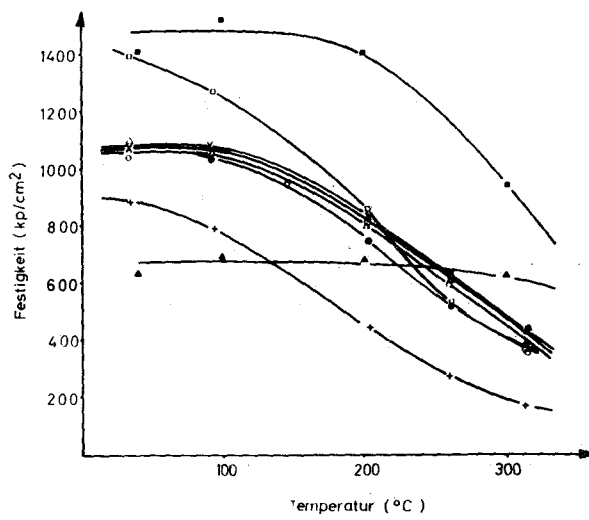
Fig. 6 : Temperature functions of calculated strength
values of UAl_3-Al cores [33]

$\times - \times - \times$ Tensile strength)   34 wt% UAl_3 in Al clad with
$o - o - o$ Yield strength   )   Al 1100

$+ - + - +$ Tensile strength   Al 1100

$\triangle - \triangle - \triangle$ Tensile strength)   50 wt% UAl_3 in Al clad with
$\bullet - \bullet - \bullet$ Yield strength   )   X 8001 Al

$\square - \square - \square$ Tensile strength   X 8001

$\blacksquare - \blacksquare - \blacksquare$ Tensile strength   (of UAl_3-Al core with 34 wt%
   (UAl_3

$\blacktriangle - \blacktriangle - \blacktriangle$ (of UAl_3-Al core with 50 wt%
   (UAl_3
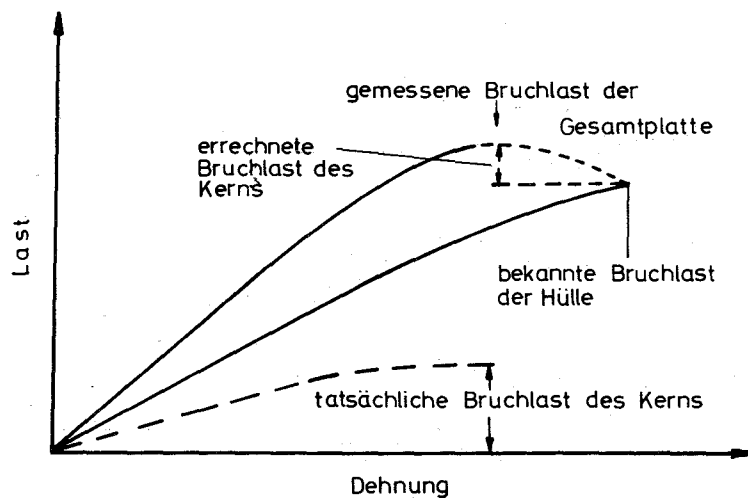
Fig. 7 : (Schematic) Conditions prevailing
during fracture
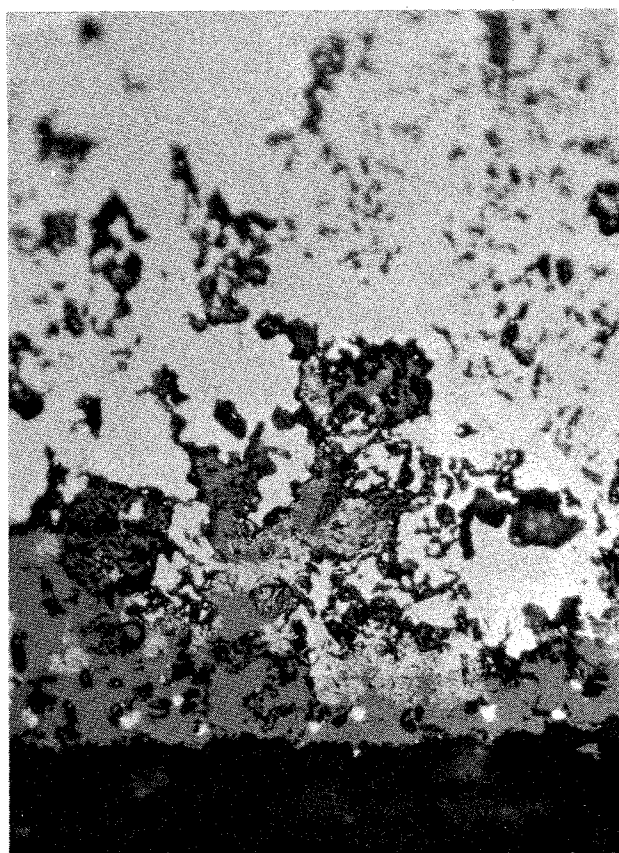
UAl_3

reaction product

Al_2O_3

Fig. 8 : Reaction of UAl_3 in "statu nascendi"
with the binder of Al_2O_3 (75 x)
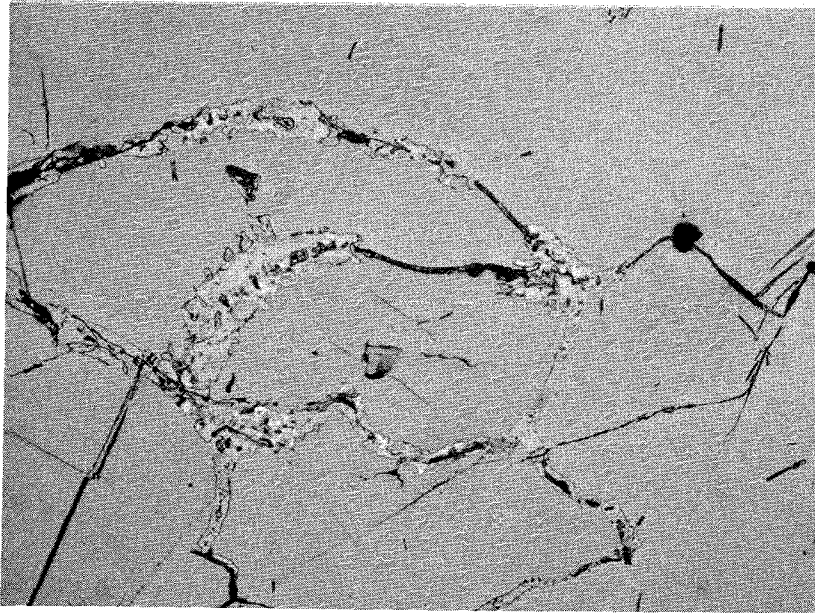
a)

b)

Fig. 9 : UAl$_3$, as cast, containing UAl$_4$ (150 x)

a) etched with nitric acid

b) unetched, polarized light
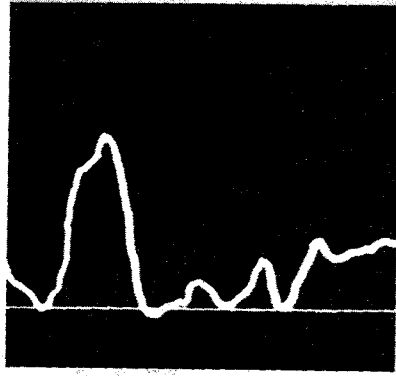
a)
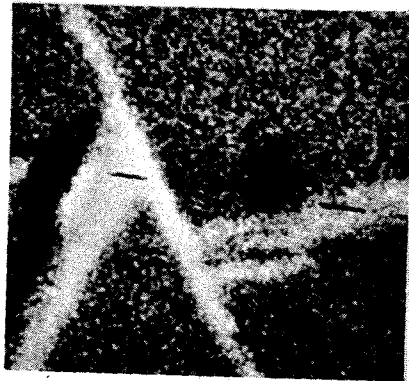
b) microprobe trace

c) microprobe trace

d)
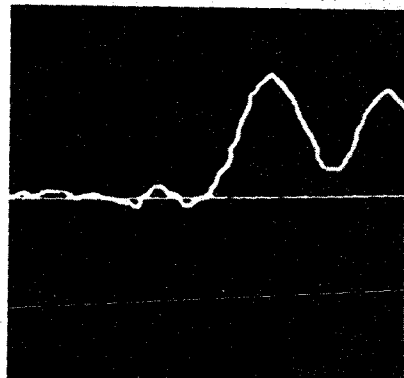
Fig. 1o : Microprobe analysis of UAl_3 prepared by melting

a, b) Al detection

c, d) U detection
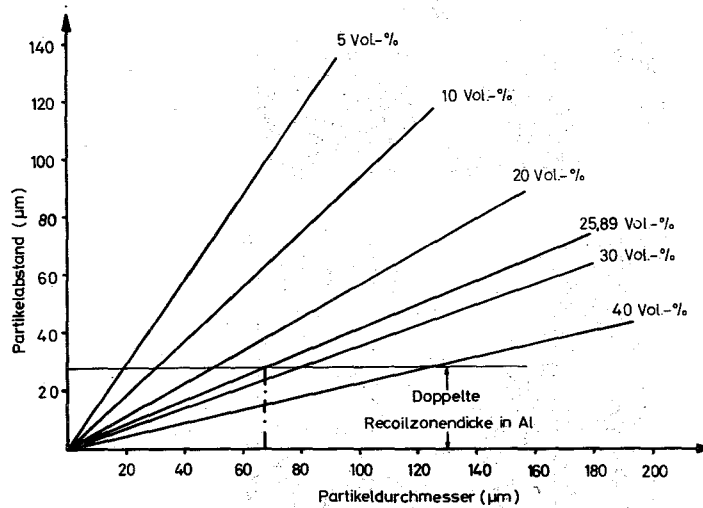
Fig. 11 : Relationship between particle diameter,
concentration, and the shortest distance
between particle peripheries for a UAl$_3$-
Al dispersion

(25.95 vol% = 51 wt% UAl$_3$)

Particle diameter (μm)	Grinding conditions		
	Grinding time = 60 sec Inserts = disc and ring in Dekalin	Grinding time = 45 sec Inserts = disc and ring in Dekalin	Grinding time = 30 sec Inserts = disc subsequently 10 sec ring in Dekalin
	Particle size distribution wt%		
> 125	15.78	18.13	54.14
125 - 90	14.70	15.04	10.49
90 - 63	18.45	14.21	8.44
63 - 45	18.45	12.38	7.33
45 - 36	11.50	6.02	4.30
< 36	21.12	34.22	15.29

Fig. 12 : Screening analysis of UAl_3 powder with variable grinding conditions
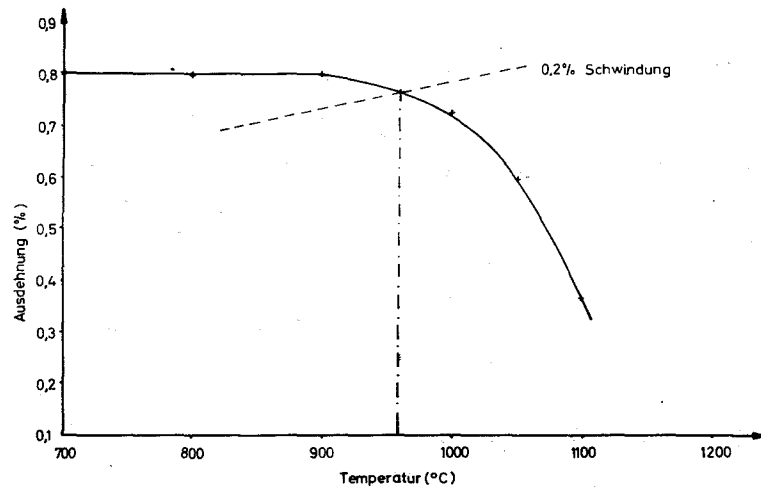
Fig. 13 : Begin of sintering of UAl$_3$ powder ($<$ 63 μm Ø)

Material	UAl$_3$ (IMF)	Al Alcoa 101
UAl$_3$ Content (wt%)	93.42	-
Al Content (wt%)	25.15	99.5
U : Al ratio (ideal 2.94)	2.88	
O$_2$ (wt%)	0.88	0.29
N$_2$ (wt%)	0.0225	
C (wt%)	0.198	
H$_2$ (wt%)	0.0088	
Fe (wt%)		0.13
Si (wt%)		0.07
Cu (wt%)		0.01
Rest (wt%)	1.13	
Particle size (μm)	63 - 125	18.6 (mean size)
Particle shape 5o : 1		
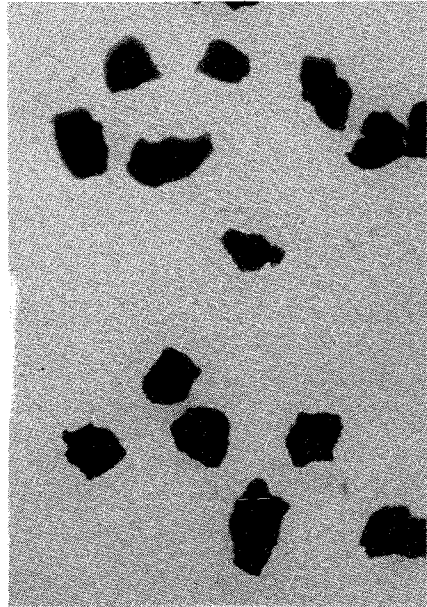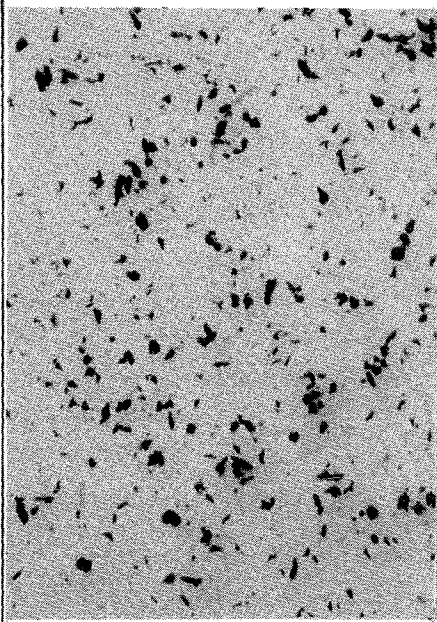
Fig. 14 : Characteristics of UAl$_3$ prepared by melting, and Alcoa 1o1 Al powders
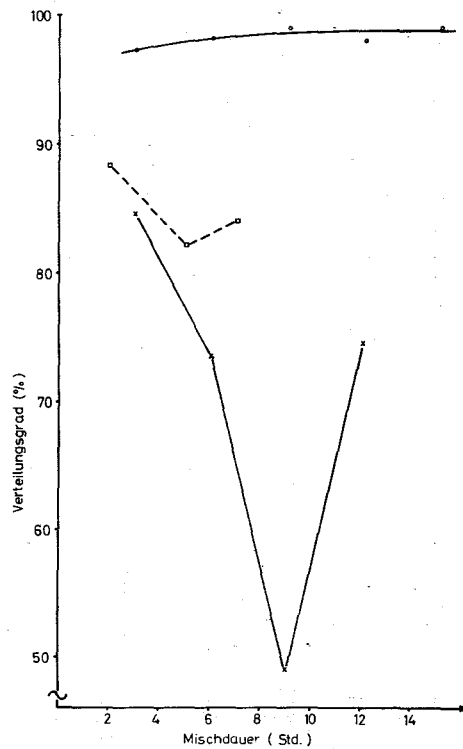
Fig. 15 : Distribution degree of UAl_3-Al powder
mixtures (2o vol% UAl_3)

o—o—o   Dry mixing; tumbler movement 7o R.p.m.
          Container vol : powder vol = 3.4

ロ—ロ—ロ   Dry mixing; tumbler movement 7o R.p.m.
          Container vol : powder vol = 6.8

x—x—x   Wet mixing (CCl_4); tumbler movement 7o R.p.m.
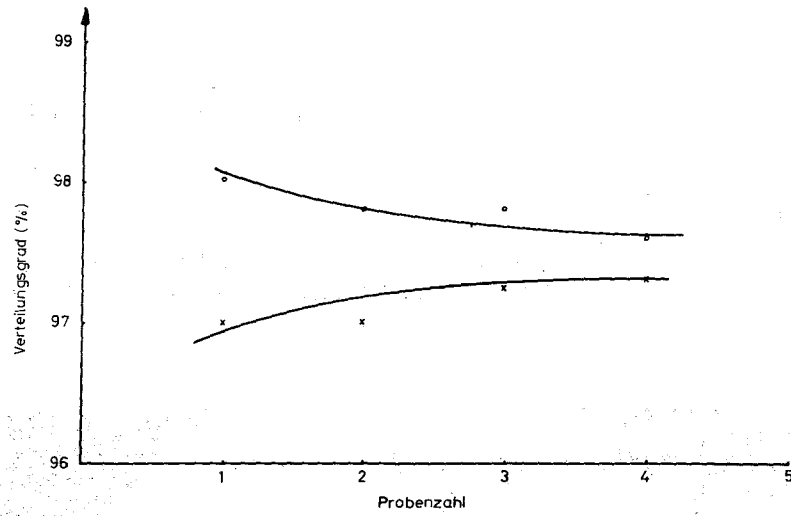
Fig. 16 : Scattering of distribution degree
          as a function of specimens analysed
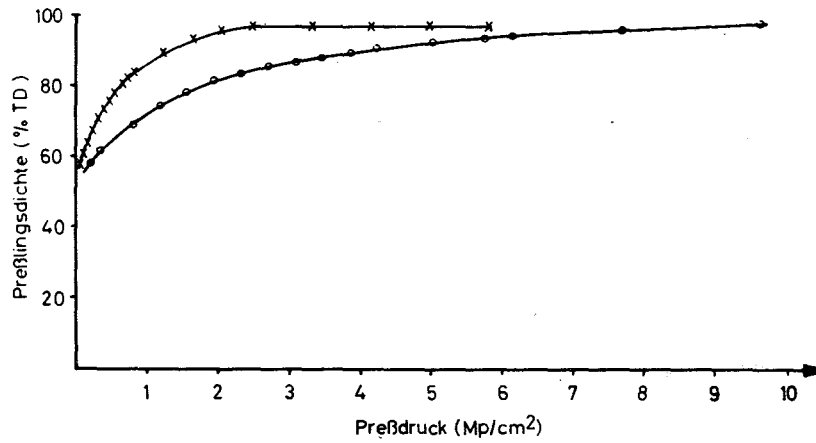
Fig. 17 : Pellet density as a function of compacting pressure
for UAl₃-Al pellets (2o vol% UAl₃) with stearin
lubricated dies

o-o-o   Cylindrical pellets pressed one sided
x-x-x   Rectangular pellets pressed on both sides
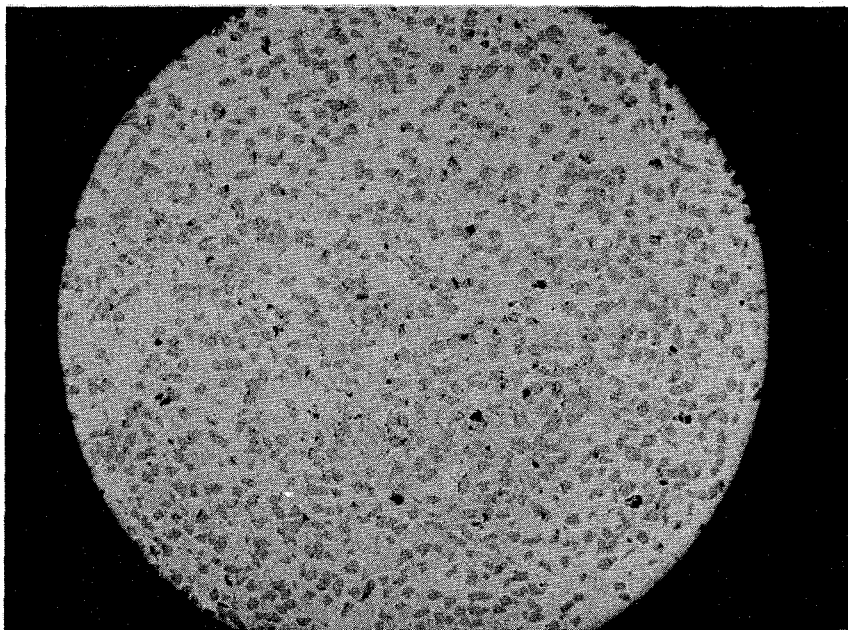
Fig. 18 : UAl₃ particles in Al matrix (2o vol% UAl₃)
(diamond polished pellet, unetched)
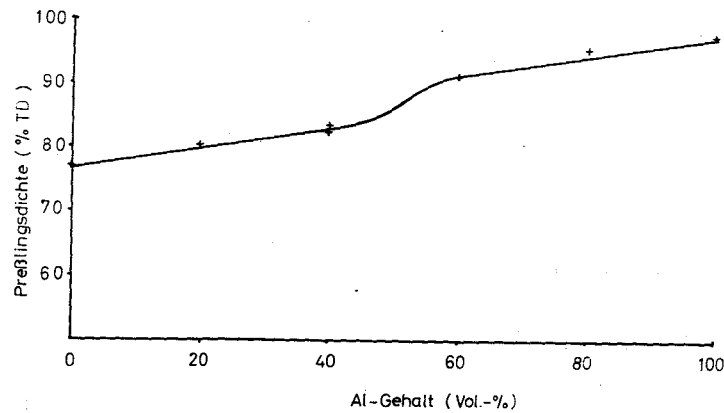
Fig. 19 : Pellet density as a function of concentration in
UAl$_3$-Al pellets (compacting pressure 5 Mp/cm^2)
height to diameter ratio = 1
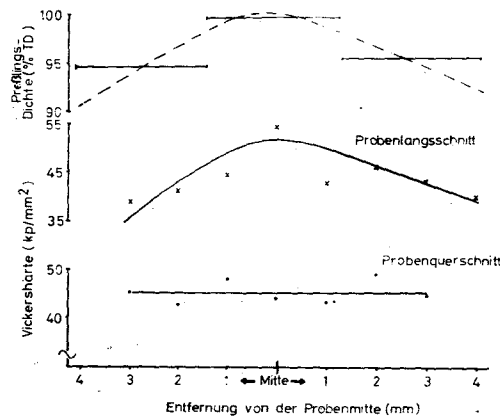
Fig. 2o : Density and hardness curves of a UAl$_3$-Al
cylindrical pellet in radial and axial directions
(height to diameter ratio = 1)
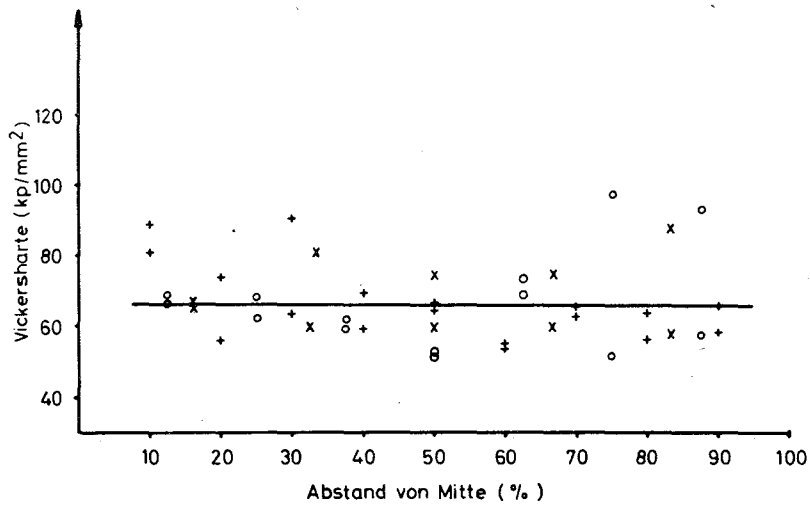
a)
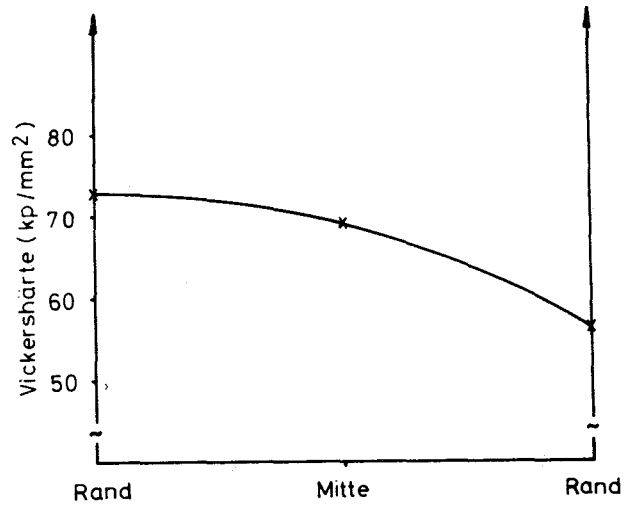
b)

Fig. 21 : Hardness curves of a UAl_3-Al rectangular
pellet
a) Surface
b) Side
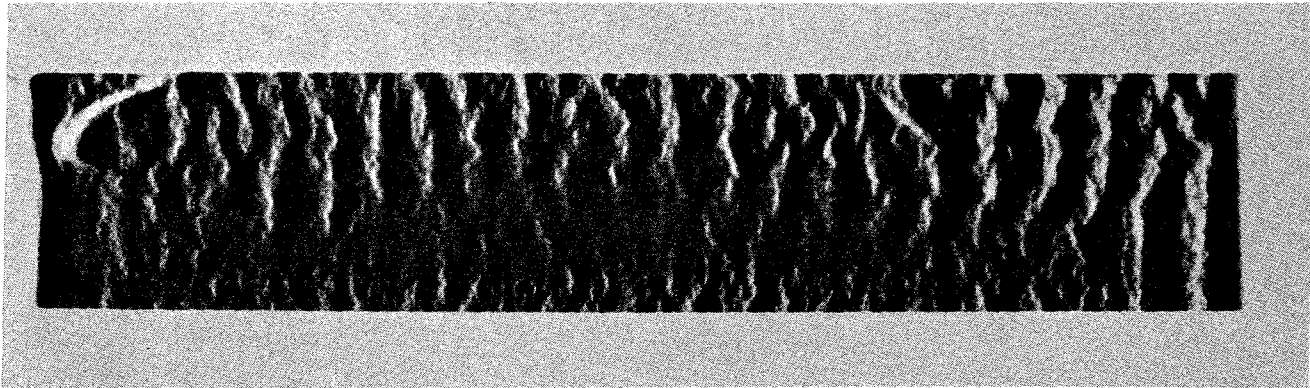
Fig. 22 : Cracks in the core as a result of density
variations in pellet

Core composition	UAl$_3$ (vol% / wt%)		25.81/46.81
	Al (vol% / wt%)		74.11/53.19
Mixing conditions	Time (hrs)		6
	Velocity (R.p.m)		7o
	Container vol : powder vol		3
Pellet dimensions (mm)			4o x 3o x 2.5
Compacting pressure (Mp/cm^2)			3.5
Picture frame material			Al (99.5)
Picture frame dimensions (mm)	Cover plates		6o x 5o x 2
	Picture frame		6o x 5o x 2.5
Irradiation test plates	Overall dimensions (mm)	Length	21o
		Breadth	4o
		Thickness	1.3
Irradiation test plates	Core Dimensions (mm)	Length	2oo
		Breadth	3o
		Thickness	o.5
Rolling conditions	Temperature (°C)		5oo
	Reduction per pass (%)		2o
	Speed of rolls (m/min)		8
	Passes per plate		7-8

Fig. 23 : Data of the picture frame technique of UAl$_3$-Al irradiation
test plates
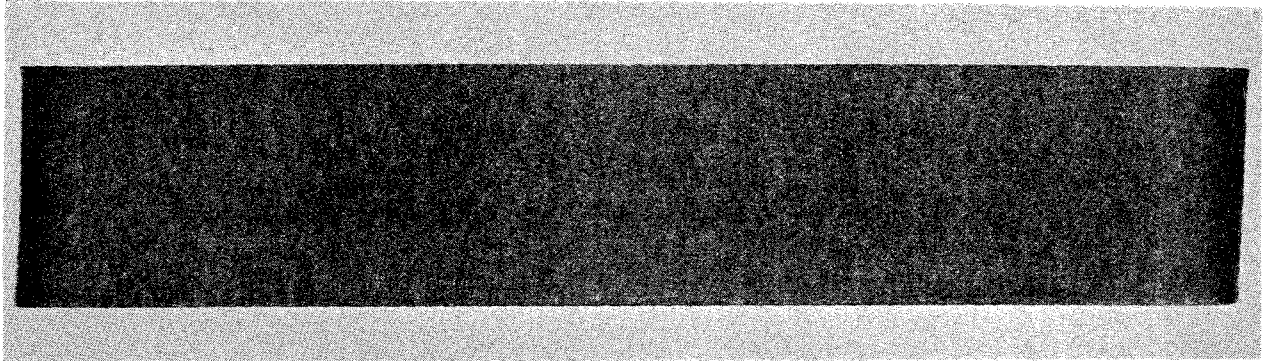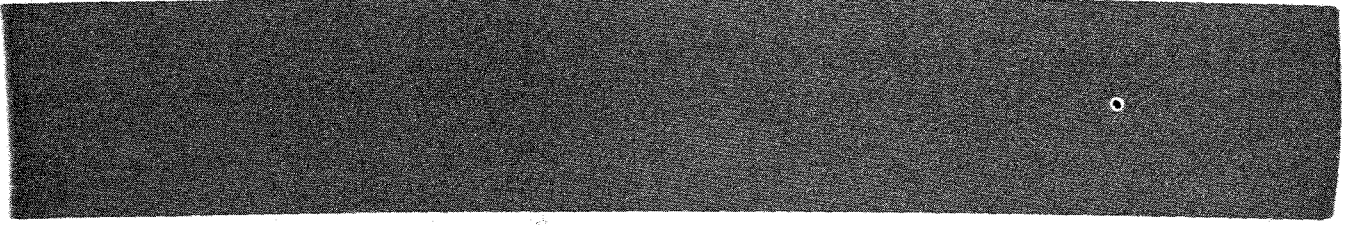
Fig. 24 : Radiographs of Al clad UAl$_3$-Al cores
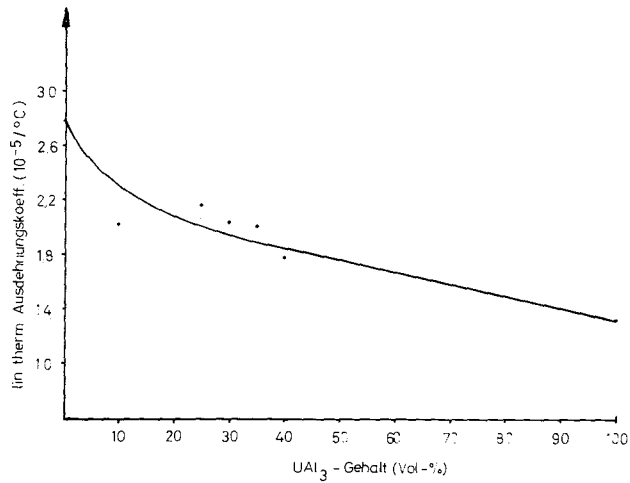
Fig. 25 : The concentration function of the thermal
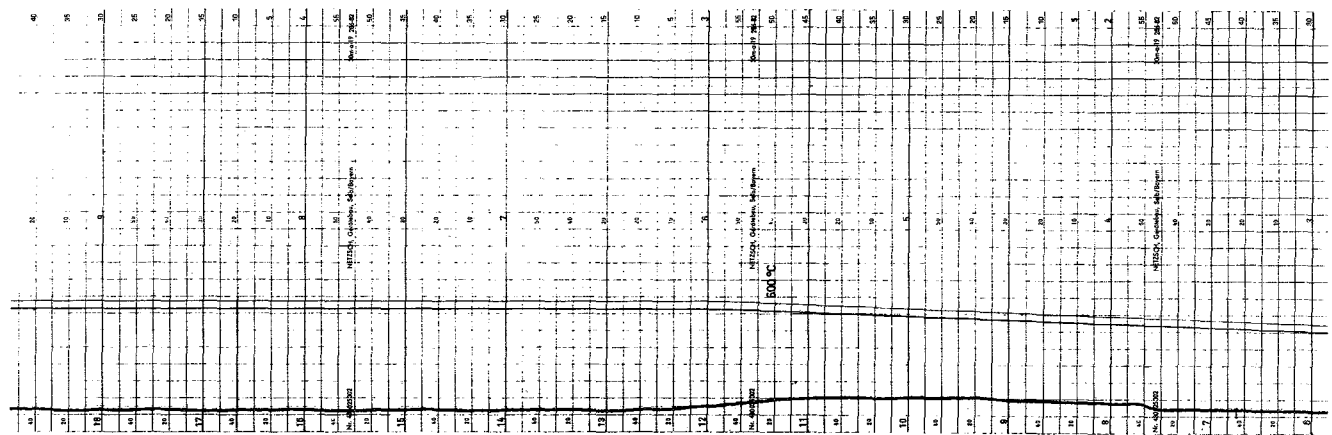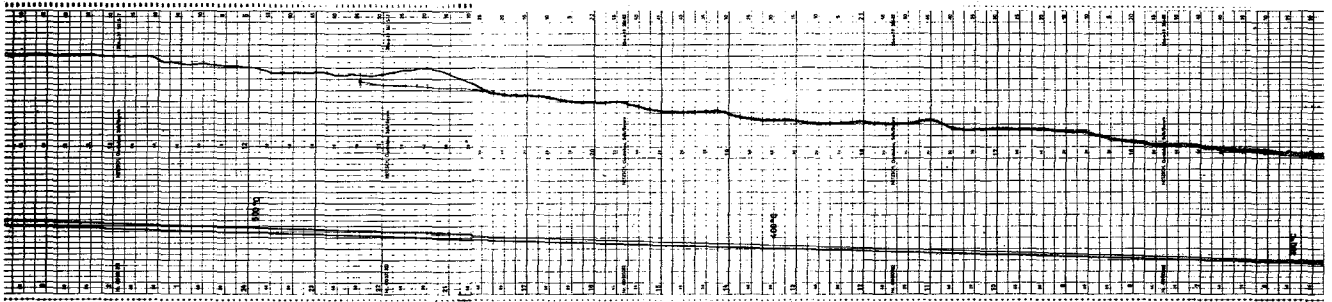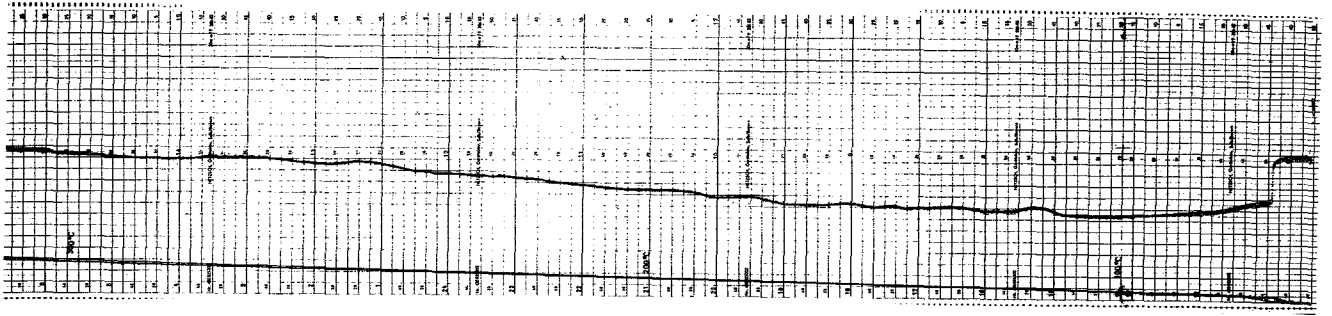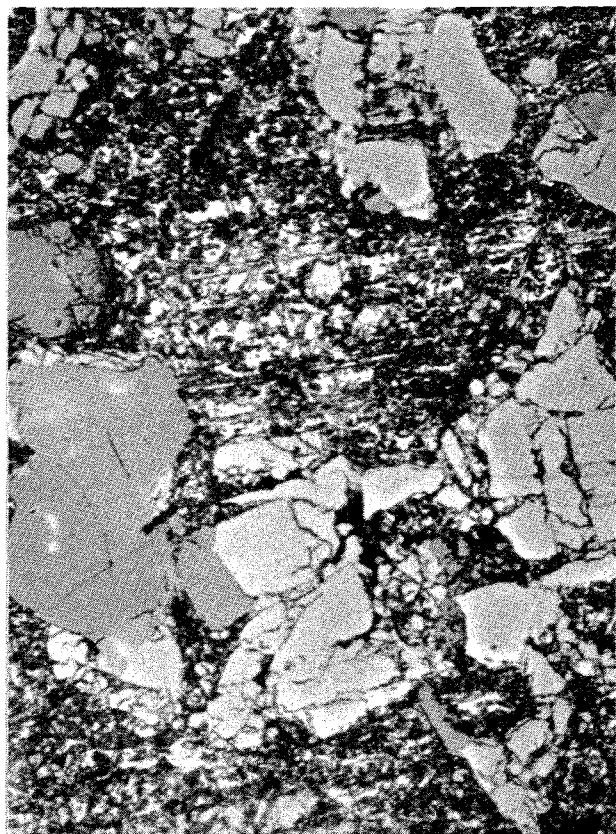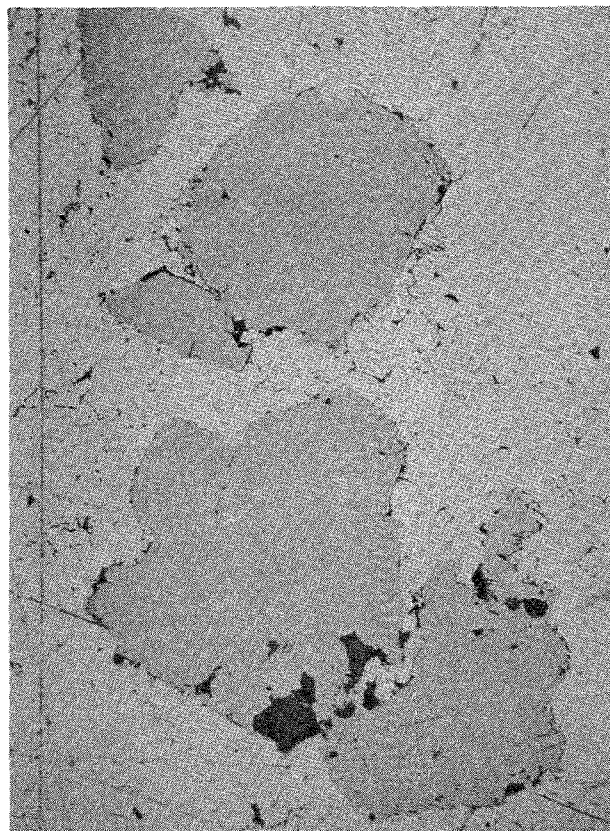expansion coefficients of UAl$_3$-Al dispersions

Fig. 26 : Signs of formation of UAl_4 during heating
of a UAl_3-Al specimen in a dilatometer

a)

b)

Fig. 27 : Microstructure showing UAl_3 and UAl_4 phases
after reaction (5oo x)

a) partial reaction, both phases
UAl_3 and UAl_4-Al present
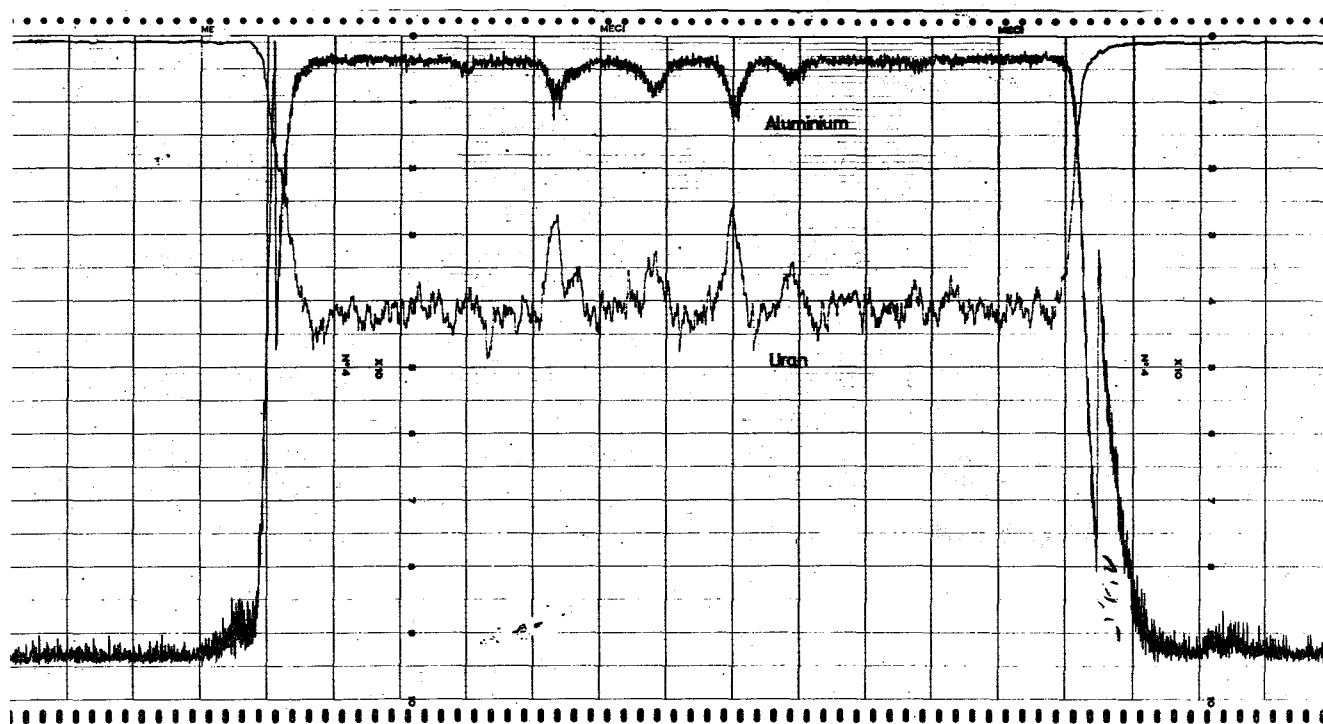
b) total reaction UAl_4 and Al present
(UAl_4 dark)

Fig. 28: Microprobe analysis of a UAl$_3$ particle
after reaction